ChemPubSoc Europe

DOI: 10.1002/cssc.201301066

CE-II

Energetics of Defects on Graphene through Fluorination

Jie Xiao,*[a] Praveen Meduri,[a, e] Honghao Chen,[a] Zhiguo Wang,[a] Fei Gao,[a] Jianzhi Hu,[a] Ju Feng,[a] Mary Hu,[a] Sheng Dai,[b, c] Suree Brown,[b, c] Jamie L. Adcock,[b, c] Zhiqun Deng,[a] Jun Liu,*[a] Gordon L. Graff,[a] Ilhan A. Aksay,[d] and Ji-Guang Zhang*[a]

Functionalized graphene sheets (FGSs) comprise a unique member of the carbon family, demonstrating excellent electrical conductivity and mechanical strength. However, the detailed chemical composition of this material is still unclear. Herein, we take advantage of the fluorination process to semi-quantitatively probe the defects and functional groups on graphene surface. Functionalized graphene sheets are used as substrate for low-temperature (<150 °C) direct fluorination. The fluorine content has been modified to investigate the formation mechanism of different functional groups such as C–F, CF_2, O–CF_2 and (C=O)F during fluorination. The detailed structure and chemical bonds are simulated by density functional theory (DFT) and quantified experimentally by nuclear magnetic resonance (NMR). The electrochemical properties of fluorinated graphene are also discussed extending the use of graphene from fundamental research to practical applications.

Introduction

Functionalized graphene sheets (FGSs) comprise highly reactive defect sites and functional groups that provide ideal substrates for further modification, such as fluorination. Fluorinated graphene has interesting physical, optical, and electronic properties and has been investigated for different applications.[1] However, its chemical composition and atomic structure are still subject to debate, especially when defects and functional groups co-exist in the graphene material undergoing the fluorination process. The delocalized electrons in graphene interact readily with the fluorine, forming graphene fluorides at low temperatures with much-improved optical properties.[2] Fluorinated graphene has also been investigated for use in electronic devices because the high electronegativity of F can be used to modulate electronic conductivity.[3]

In spite of the research work described above, details of the structural transition from FGSs to functionalized fluorinated graphene remain unclear.[4] The origin and the evolution of C–F structures, molecular-level interactions between fluorine and defects/functional groups, and the electrochemical properties of fluorinated graphene have not been previously explored in the presence of defect sites and functional groups. In fact, the fluorination process may provide a unique way to semi-quantitatively probe the defects and functional groups present in a graphene, given that fluorinated defective sites have different signals that can be accurately discerned by, for example, nuclear magnetic resonance (NMR) spectroscopy. Studying the fluorination mechanism of FGSs not only enhances our understanding of the chemical information on the surface, but also provide a useful approach to probe into the parent FGS materials.

In the present study, we used FGSs (Vorbeck Materials, Jessup, MD, USA) with a C/O ratio of 14 as substrate and implemented low-temperature (<150 °C) direct fluorination of graphene sheets.[5] The fluorine content was modulated during the fluorination process to investigate the mechanisms by which different functional groups, such as C–F, CF_2, O–CF_2 and (C=O)F, are formed. The detailed structure and chemical bonds were simulated by density functional theory (DFT) and quantified experimentally by NMR. These DFT and NMR studies revealed that lattice vacancies, without oxygen-containing groups, provide most of the reactive sites that react with F at the onset. FGSs also contain COOH, hydroxyl, and epoxy groups that contribute to the reaction products at higher F contents. We emphasize that this study provides direct information useful for optimizing the energy and power density for energy storage in electrode materials.

[a] Dr. J. Xiao,[+] Dr. P. Meduri,[+] H. Chen, Dr. Z. Wang, Dr. F. Gao, Dr. J. Hu, Dr. J. Feng, M. Hu, Dr. Z. Deng, Dr. J. Liu, Dr. G. L. Graff, Dr. J.-G. Zhang
Pacific Northwest National Laboratory
Richland, WA 99352 (USA)
E-mail: jie.xiao@pnnl.gov
ji-guang.zhang@pnnl.gov
jun.liu@pnnl.gov

[b] Dr. S. Dai, Dr. S. Brown, Dr. J. L. Adcock
The University of Tennessee
Knoxville, TN 37996 (USA)

[c] Dr. S. Dai, Dr. S. Brown, Dr. J. L. Adcock
Chemical Sciences Division
Oak Ridge National Laboratory
Oak Ridge, TN 37831 (USA)

[d] Dr. I. A. Aksay
Department of Chemical and Biological Engineering
Princeton University
Princeton, NJ 08544 (USA)

[e] Dr. P. Meduri[+]
Present address:
Department of Materials Science & Engineering
Pennsylvania State University
University Park, PA 16802 (USA)

[+] These authors contributed equally to this work.

CE-II Part of a Special Issue on "The Chemistry of Energy Conversion and Storage". To view the complete issue, visit: http://onlinelibrary.wiley.com/doi/10.1002/cssc.v7.5/issuetoc.

 © 2014 Wiley-VCH Verlag GmbH & Co. KGaA, Weinheim

Results and Discussion

Three different graphene fluorides were synthesized to investigate the evolution of chemical bonding between C and F, with fluorine contents of 0.47, 0.66, and 0.89. To quantify the relative amounts of functional groups on the parent FGSs, ^{19}F magic-angle spinning (MAS) NMR spectra were acquired at a sample spinning rate of 22 kHz from freshly synthesized CF_x samples (Figure 1 a). The $CF_{0.89}$ sample spectrum shows five distinct peaks with chemical shifts of −178 ppm (peak 1), −121 ppm (peak 2), −116 ppm (peak 3), −83 ppm (peak 4), and −72 ppm (peak 5). These chemical shifts can be assigned as follows:[6] peak 1 (−178 ppm) corresponds to covalently bonded C–F structures; peaks 2 and 3 (−121 and −116 ppm) correspond to $-CF_2-$ structures; peak 4 (−83 ppm) corresponds to $-O-CF_2-$, overlapping partially with one peak from $-CF_3$; and peak 5 (−72 ppm) also corresponds to the $-CF_3$ structure. Peak 6, at 57 ppm in samples $CF_{0.66}$ and $CF_{0.47}$, most likely corresponds to –(C=O)F structures. The sharp peak 2 in samples CF0.66 and CF0.47 can be explained by significant random molecular or segmental motion, the intensity of which is reduced in the high-F-content sample CF0.89. Peak 3 (−116 ppm) corresponds to rigid CF_2 structures, based on its broad line width compared to peak 2.

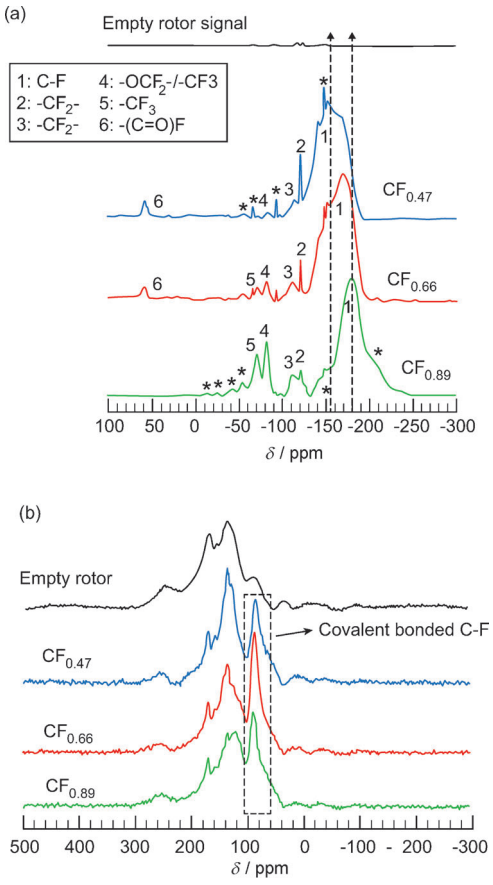

Figure 1. NMR spectra acquired at a sample spinning rate of 22 kHz of freshly synthesized CF_x samples, where $x = 0.47$, 0.69, and 0.89. (a) ^{19}F MAS spectra of CF_x and a back ground ^{19}F spectrum acquired on an empty rotor with 30 000 scans. Peaks denoted by "*" are sample spinning sidebands. (b) ^{13}C MAS spectra of CF_x and a background scan.

The line width of peak 1 broadens as the peak shifts to higher ppm values, from −178, to −170, to −150 with a decrease in the fluorine content from $CF_{0.89}$, to $CF_{0.66}$, to $CF_{0.47}$, respectively, which indicates an increasingly diverse set of CF structures presumably formed from different defects of FGS (discussed in more detail later). Meanwhile, with increasing F coverage the relative intensity of peak 6, corresponding to –(C=O)F–, decreases, approaching zero in $CF_{0.89}$. This is related to further fluorination from –(C=O)F to $-OCF_2-$ and, likely, CF_3, as will be discussed in the section on modeling. In contrast, the intensities of peaks 4 ($-OCF_2-/-CF_3$) and 5 ($-CF_3$) increase, indicating a significant increase in the relative amounts of these structures when the F content is increased. To further validate the formation of covalently bonded C–F structures, ^{13}C MAS NMR spectra were measured, and these are shown in Figure 1 b. Peaks corresponding to covalently bonded C–F can be clearly observed in the spectra of the CF_x samples, with a distinct peak centered at 86 ppm. ^{13}C peaks corresponding to the various functional groups, such as CF_2, CF_3, and $-OCF_2-$ and (C=O)F, are difficult to observe, primarily because of heavy overlap with the background signal as well as the relatively low abundance of these functional groups. Notably, fluorination on sites other than defect or functional group ones always occurs through bonding with π electrons; a well-documented phenomenon in graphite fluorination processes. However, in this work, we only discuss the order of the interactions between F and various defective sites in an attempt to quantify the defects by using F as a molecular tag.

To obtain information on the mechanism of the fluorination process, the migration of F and the formation energies of different chemical bonds during fluorination were calculated based on DFT.[7] The energy barrier of F migration on graphene was determined as ca. 0.28 eV. This low energy barrier allows F to migrate to the defects and edges containing functional groups at room temperature. This is consistent with recent ab initio molecular dynamics simulations, showing that graphene with carbon vacancies is an effective catalyst for nitromethane combustion.[8] Thus, fluorination occurring on these sites is considered.

Vacancy defects and functional groups were modeled by using a periodic super cell of rhombus-shaped graphene with side-length of 24.62 Å, containing 200 carbon atoms with a divacancy, and with atoms at the edge of the divacancy saturated by F only (as shown in Figure 2) or the functional groups of –H, –O, –OH, and –COOH. A study of vacancy defects in graphene suggested that a divacancy is more stable than a single vacancy, and is a common active site.[9] A divacancy can be created by the coalescence of two monovacancies, forming a fully reconstructed V2(5-8-5) divacancy, as demonstrated by tight-binding or ab initio molecular dynamics simulations.[10] Also, the transformation from V2(5-8-5) to other divacancy configurations can be triggered by electron irradiation.[11] In the present study, we consider only a V2(5-8-5) configuration. Vacuum is applied up to a distance of 30 Å between graphene layers to avoid interaction between graphene and its images due to the

© 2014 Wiley-VCH Verlag GmbH & Co. KGaA, Weinheim

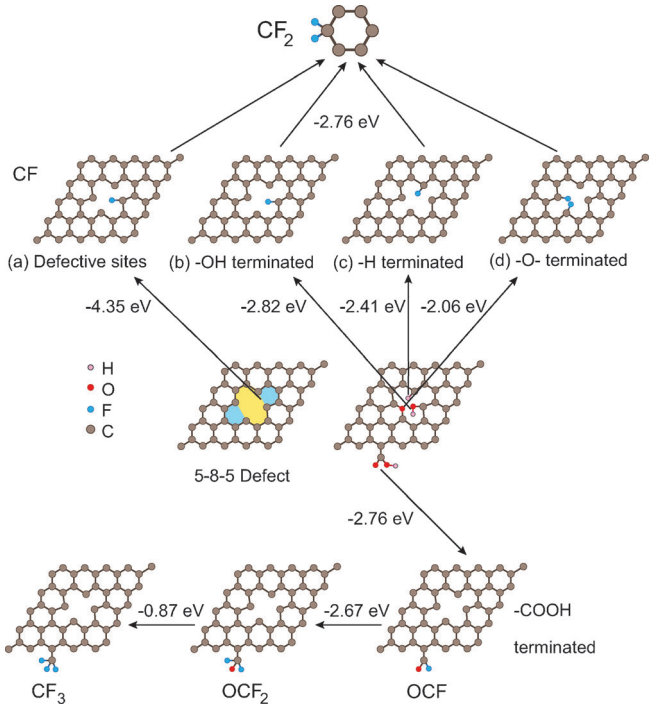

Figure 2. Simulation of fluorination on a graphene substrate containing different defective sites in a divacancy and functional groups, along with the individual formation energies of C–F bonds at different stages.

periodic boundary conditions along the normal direction of graphene.

The formation energy of F at the edge E_f^F was calculated by using:

$$E_f^F = [E_R - E_{ini} - NE_F]/N \quad (1)$$

where E_R and E_{ini} are the total energies of a system after and before fluorination, respectively.

The formation energies of F with functional groups were determined by:

$$E_f = [E_R - E_{ini} - NE_F + ME_X]/N \quad (2)$$

where E_X is the energy of –H, -OH, or –O, and E_F is the energy of F. N and M are the numbers of F replacing –H, –OH, or –O, respectively.

E_{OH} was defined with respect to H_2-rich conditions; that is:

$$E_{OH} = E_{H_2O} - \frac{1}{2}E_{H_2} \quad (3)$$

where E_{H_2} and E_{H_2O} are the total energies of the H_2 and H_2O molecules, respectively.

Figure 2 shows the formation of a C–F bond at the V2(5-8-5) divacancy and defective sites associated with –OH, –O–, or –H functional groups, along with their individual formation energy calculated by using Equation (1). Fluorination of a –COOH group at the edges of graphene is also shown in Figure 2. All formation energies during the fluorination processes are negative, indicating that they are exothermic and occur spontaneously. Energetically, the most favorable configuration is the binding of F on the edge defect site due to the unsaturated nature of the dangling carbon bond, with the lowest formation energy of −4.35 eV among all the possible reactions (Figure 2a). Thus, this process leads to the formation of a CF structure. Notably, the second-lowest formation energy (−2.82 eV) is for F to replace –OH (Figure 2b). This process may also contribute to the formation of CF structures, especially at higher temperatures. The results from –O– or –H groups to form CF are similar to that from –OH group, as indicated in Figure 2c–d. With the increase of F coverage, CF can be further fluorinated to CF_2, with a formation energy of −2.76 eV (Figure 2). However, the relative fraction of CF should be larger than CF_2 due in part to the lower formation energy of CF, depending on F coverage. According to the formation energies of other configurations, it is also possible that COOH can be fluorinated to OCF at intermediate F coverage and then to OCF_2 at increasing F coverage, as shown in Figure 2. These results show excellent agreement with the occurrence of OCF, CF_2 and OCF_2 groups in the NMR spectrum for $CF_{0.47}$. As the formation energy of $OCF_2 + F \rightarrow CF_3 + O$ is higher than other fluorination processes, CF_3 can be formed only at higher F coverage and higher temperatures, which also agrees well with the experimental results showing the presence of CF_3 groups in $CF_{0.66}$ and $CF_{0.89}$ samples.

A quantification of functional groups on parent graphene obtained from the spectrum in Figure 1 is shown in Table 1. The relative total peak area of the background signal is defined as "1". All other values are expressed relative to the background signal. The conditions were kept identical, with peak area normalization per unit weight and per unit accumulation number for quantitative analysis. For $CF_{0.19}$, where F coverage is the lowest, the CF structure dominates. This NMR result of 100% CF at low F coverage ($CF_{0.19}$) is in agreement with DFT simulations, which elaborate the formation of CF structure on the defects in the earlier discussion. At this early stage (low F coverage), almost all of those C–F single bonds in $CF_{0.19}$ should

Table 1. Quantitative data obtained from ^{19}F MAS NMR spectra in Figure 1.[a]

Sample	Total area		CF	CF_2		(C=O)F	O–CF_2/CF_3	CF_3	CF/all
	per scan	per mg[b]		rigid	mobile				structures
background	1	N/A	N/A	N/A	N/A	N/A	N/A	N/A	N/A
$CF_{0.19}$ (aged)	3.3	5.2	5.2	0	0	0	0	0	100%
$CF_{0.47}$ (fresh)	52	34.2	30.5	1.4	0.8	1.0	0.5	0	89%
$CF_{0.66}$ (fresh)	76	44	37.6	2.0	0.5	1.1	1.9	0.9	85.4%
$CF_{0.89}$ (fresh)	213	100	78	6.4	0.2	0	7.5	7.8	78%

[a] CF refers to "C–F" single bond; CF_2 is a carbon that has two F atoms attached in the form of F–C–F; CF_3 is a carbon that has three F atoms attached; (C=O)F means that the carbon has one F atom (single bond to C) and one O (double bond to C) attached. O–CF_2 is a carbon that has one O atom (single bond) and two F atoms (each with a single bond to C) attached. O–CF_3 is a carbon that has one O (single bond) atom and three F atoms (each with a single bond to C) attached. [b] Free from background.

© 2014 Wiley-VCH Verlag GmbH & Co. KGaA, Weinheim

be formed from those defect sites. Further increase of C–F bonding to 30.5% in the case of $CF_{0.47}$ only leads to a slight increase of CF_2 structures (1.4+0.8=2.2%). At this stage, the defect sites should still be the dominant reaction sites for F due to the low formation energy. Some functional groups (hydroxyl of epoxy) may also contribute to the formation of CF_2, but their contribution is small and cannot be distinguished from the contribution of the CF_2 formed at the defect sites based on similar energetics. (C–O)F formed at this stage can only be derived from the carboxylic group (COOH) based on the calculations. In $CF_{0.89}$, the number of C–F single bonds in CF and CF_2 has been increased to 78% and 6.4+0.2=6.6%, respectively. Meanwhile, (C=O)F decreases to zero, indicating that most of the defect sites without functional groups have been exhausted during fluorination at this stage.

Based on the above discussions, the content of defect sites without any functional group is estimated to be between 37.6 and 78%. These results are consistent with literature reports stating that FGSs or reduced graphene oxides contain a large array of complex defect sites.[12] This study also confirms the existence of COOH groups in the FGSs, which give rise to the formation of OCF_2 or OCF_3, and eventually CF_3 groups. Simple compositional analysis suggests that these reactions need 2.5% to 3.75% O-containing groups. The FGS sample we used has a C/O ratio of 14, or O content of 7.1%. Considering that hydroxyl and epoxy groups also participate in the reaction, FGS should roughly contain an additional ca. 3.35% hydroxyl or epoxy groups. To the best of our knowledge, there is no report on the combination of fluorination processes with NMR analysis to quantify the relative amount of different functional groups on graphene. This strategy is an important complement to the Raman or X-ray photoelectron spectroscopy (XPS) techniques. The latter are widely adopted for defect quantification but their results vary, potentially due to the sophisticated surface chemistry of functionalized graphene as well as the limit of the spectroscopic methods.

The defects and functional groups on the surface also have a large effect on the charge storage and transport properties. To further correlate the fluorination process of graphene with the final electrochemical properties of graphene fluorides, as-prepared CF_x (x=0.47, 0.66, 0.89) samples were tested as cathode materials in lithium batteries. The discharge profiles of the different graphene fluorides at C/5 rate are presented in Figure 3a. The theoretical open circuit voltage (OCV) for the overall reaction: Li+CF→LiF+C calculated thermodynamically is 4.57 V.[13] However, the real OCV is slightly over 3.0 V for the stoichiometric CF material with an initial voltage delay during discharge and an operational voltage of 2.4~2.5 V.[14] The discharge plateau for $CF_{0.47}$ shown in Figure 3a is ~2.7 V at C/5 rate with a specific capacity of ~469 mA h g^{-1}.

The increase in the operational voltage in $CF_{0.47}$ can be correlated to the faster diffusion of solvated Li^+ in all directions on graphene nanosheets with a reduced number of surface groups such as CF_2 or CF_3, which may impede prompt Li^+ transport. The discharge for $CF_{0.89}$ and $CF_{0.66}$ starts with an initial voltage delay and a sloping profile occurs from 2.3 and 2.4 V with specific capacities of ~554 mA h g^{-1} and

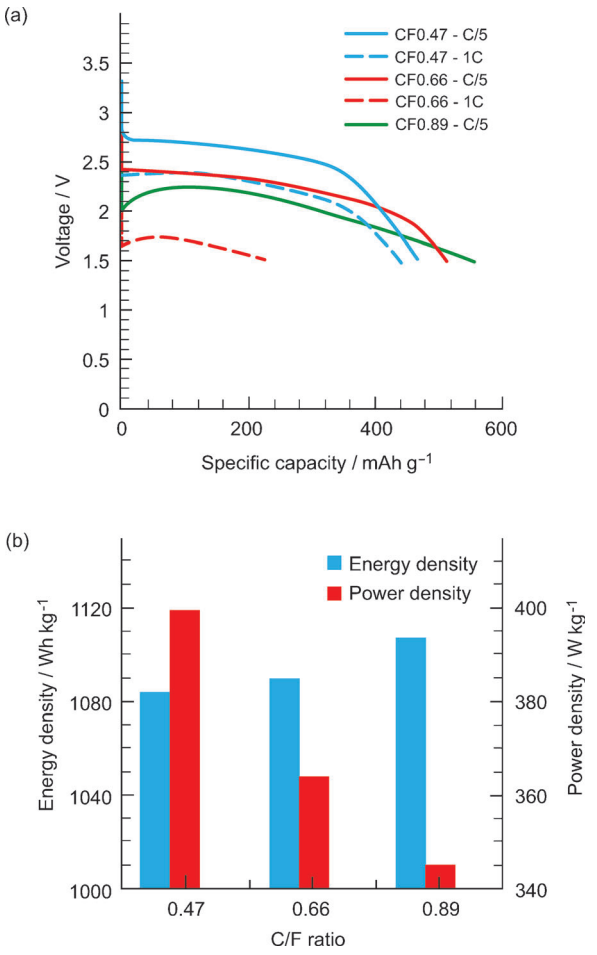

Figure 3. (a) Rate performance of fluorinated graphene materials (1C current density for $CF_{0.47}$—602 mA g^{-1}; $CF_{0.66}$—721 mA g^{-1}; $CF_{0.89}$—825 mA g^{-1}). (b) Comparison of gravimetric energy and power densities of fluorinated graphene at C/5 rate.

~517 mA h g^{-1} at a rate of C/5, respectively. The specific capacity of the fluorinated graphene materials is directly related to the fluorine content in CF_x, since the discharge product is LiF (and carbon). When the rate is increased to 1C, both capacity (240 mA h g^{-1}) and operating voltage (1.7 V) drop greatly for $CF_{0.66}$ as shown in Figure 3a while $CF_{0.89}$ cannot be discharged at all. However, $CF_{0.47}$ still delivers a capacity of more than 400 mA h g^{-1}. The reason is due to the increased surface groups (CF_2, CF_3) on $CF_{0.66}$ or $CF_{0.89}$ that lead to slow diffusion of solvated Li^+ especially at high rates.

The lower amounts of unreacted graphene with reduced in-plane conductivity also contribute to the poor rate performance observed with increasing F coverage. Figure 3b compares the gravimetric energy and power densities of these materials at C/5. It can be seen that the energy density is the highest for $CF_{0.89}$ at C/5 rate, whereas at the same rate the power density is the highest for $CF_{0.47}$. Similarly, $CF_{0.47}$ has good energy and power density at 1C, which indicates that the fluorine content on graphene can be tuned to obtain appropriate energy/power density.

© 2014 Wiley-VCH Verlag GmbH & Co. KGaA, Weinheim

Conclusions

The chemical composition and structural evolution of graphene during fluorination were investigated by a combination of experiments and simulations. The gradual peak transitions, reflecting the nature of chemical bonding, from ^{19}F and ^{13}C MAS NMR were elaborated by using DFT calculations. It was proposed that upon fluorination, F atoms migrate easily to the vacancy sites due to low energy barrier and prefer to react with the defects without any functional groups to form C–F single bonds.

Quantification of graphene defects was executed based on this combined strategy, provides a rough assessment of defect sites without functional groups. This study helps to optimize properties of electrode materials. The energy/power ratio of as-prepared fluorinated graphene is tunable by modifying the C/F ratio, demonstrating both an informative fundamental phenomenon as well as a promising practical use for energy storage. Although it is hard to quantify each single-bonded functional group (i.e., –OH, –O–, and –H) exactly, functional groups with C=O double bonds such as –COOH are clearly differentiated and quantified by NMR analysis in this study.

Experimental Section

FGSs (Vorbeck Materials) were prepared by using thermal expansion of graphite oxide with a C/O ratio of 100.[5] The fluorination of FGS was carried out in 7% *v/v* of fluorine (F_2)/helium (He) gases for one day followed by gradual rise of F_2 in about 1–2 h, to 100% when the helium was shut off on the second day. $CF_{0.89}$, $CF_{0.66}$, and $CF_{0.47}$ were synthesized at temperatures of 150 °C, 75 °C, and room temperature (25 °C), respectively. The reactor was weighed before and after fluorination to obtain the C/F ratio. It was assumed that the weight loss due to the volatile product formation was negligible and that all the weight gained was due to F addition.

The ^{19}F and ^{13}C MAS NMR experiments were performed on a Varian-Agilent 89 mm wide-bore 850 MHz NMR spectrometer. The main magnetic field was 19.964 Tesla and the corresponding ^{19}F and ^{13}C Lamor frequencies were 799.796 and 213.733 MHz, respectively. A commercial 3.2 mm XFH pencil-type MAS probe was used for acquiring both the ^{19}F and the ^{13}C spectra at room temperature. About 18 to 31 mg of samples was used for each measurement and a sample spinning rate of about 22 kHz ± 5 Hz was used. A single-pulse sequence was used for the measurement of 19F with a recycle delay time of 1 s. The number of scans varied between 886 and 30000. The chemical shifts of ^{19}F spectra were referenced to CCl_3F (0 ppm). Similarly, a single-pulse sequence with gated proton high power decoupling during data acquisition was used for the measurement of ^{13}C with a recycle delay time of 5 s and the number of scans varied between 10000 and 30000. The chemical shifts of ^{13}C were referenced to TMS (0 ppm).

The slurry used for the coating was prepared using 85 wt% of active material, 10 wt% of Super P carbon, and 5 wt% of polyvinylidene fluoride (PVDF) mixed in *N*-methyl-2-pyrrolidone. The slurry was cast onto an aluminum foil using a Hohsen corporation MC10 coater. The cast thin film was ca. 20 μm thick with a loading of ca. 1–1.5 mg cm^{-2}. The coated film was then punched into electrodes and vacuum-dried at 70 °C overnight. Coin cell assembly was carried out in an argon environment glove box (MBRAUN, Inc.). 1 M $LiPF_6$ in a 1:2 (*v/v*) mixture of ethylene carbonate (EC) and dimethyl carbonate (DMC) was used as the electrolyte. An Arbin BT-2000, 96-channel battery tester was used to obtain the charge/discharge characteristics of electrodes which were discharged to 1.5 V at different current densities/discharge rates (1C = 864 mA g^{-1}).

All of the calculations were performed by using density functional theory, within local density approximation using the Ceperly–Alder parameterization[15] as implemented in the SIESTA code,[16] which adopts a linear combination of numerical localized atomic orbital basis sets for the description of valence electrons and norm-conserving nonlocal pseudo potentials for the atomic core.[17] The valence electron wave functions were expanded using double-ζ basis plus polarization set. The charge density was projected on a real space grid with a cutoff of 200 Ry to calculate the self-consistent Hamiltonian matrix elements. The migration barrier calculations of F on graphene was performed using the nudged elastic band (NEB) method[7a] as implemented in the Vienna ab initio package (VASP)[4a] with a plane-wave basis set. The projector augmented wave (PAW) method[7c] was used to describe electron-ion interaction, while the generalized gradient approximation using the Perdew–Burke–Ernzerhof (PBE) function was used to describe the electron exchange-correlation. A plane wave basis set up to an energy cutoff of 400 eV was used. In NEB, the initial and final states were first relaxed to make sure that the minimum energy configurations were achieved. The transition state search began with an NEB calculation, which involves a chain of images (8 in the present calculations) initially determined through linear interpolation from the fixed initial and final states.

Acknowledgements

This research was supported by the U.S. Department of Energy (DOE), Office of Basic Energy Sciences, Division of Materials Sciences and Engineering under Award KC020105-FWP12152 and was conducted at the Pacific Northwest National Laboratory (PNNL) which is operated by Battelle for DOE under Contract DE-AC05-76L01830. The modeling and NMR work were performed at the Environmental Molecular Sciences Laboratory (EMSL), a national scientific user facility sponsored by (DOE) Office of Biological and Environmental Research, located at PNNL. The fluorination was conducted at UTK and sponsored by the DOE, Office of Basic Energy Sciences, Division of Materials Sciences and Engineering. The authors also thank Ms. Yunya Dai for the help in plotting the modeling figures.

Keywords: density functional calculations · energy storage · fluorine · graphene · NMR spectroscopy

[1] a) F. Karlický, K. K. R. Datta, M. Otyepka, R. Zbořil, *ACS Nano* **2013**, *7*, 6434–6464; b) E. D. Grayfer, V. G. Makotchenko, L. S. Kibis, A. I. Boronin, E. M. Pazhetnov, V. I. Zaikovskii, V. E. Fedorov, *Chem. Asian J.* **2013**, *8*, 2015–2022; c) S.-H. Cheng, K. Zou, F. Okino, H. R. Gutierrez, A. Gupta, N. Shen, P. C. Eklund, J. O. Sofo, J. Zhu, *Phys. Rev. B* **2010**, *81*, 205435; d) A. K. Geim, *Science* **2009**, *324*, 1530–1534; e) F. Withers, S. Russo, M. Dubois, M. F. Craciun, *Nanoscale Res. Lett.* **2011**, *6*, 526.

[2] J. T. Robinson, J. S. Burgess, C. E. Junkermeier, S. C. Badescu, T. L. Reinecke, F. K. Perkins, M. K. Zalalutdniov, J. W. Baldwin, J. C. Culbertson, P. E. Sheehan, E. S. Snow, *Nano Lett.* **2010**, *10*, 3001–3005.

[3] a) J. C. Charlier, X. Gonze, J. P. Michenaud, *Phys. Rev. B* **1993**, *47*, 16162–16168; b) W. H. Lee, J. W. Suk, H. Chou, J. Lee, Y. Hao, Y. Wu, R. Piner, D. Akinwande, K. S. Kim, R. S. Ruoff, *Nano Lett.* **2012**, *12*, 2374–2378.

[4] a) H. Şahin, M. Topsakal, S. Ciraci, *Phys. Rev. B* **2011**, *83*, 115432; b) O. Ruff, Z. O. Bretschneider, *Z. Anorg. Allg. Chem.* **1934**, *217*, 1–18; c) F.

© 2014 Wiley-VCH Verlag GmbH & Co. KGaA, Weinheim

Withers, T. H. Bointon, M. Dubois, S. Russo, M. F. Craciun, *Nano Lett.* **2011**, *11*, 3912 – 3916.
[5] a) H. C. Schniepp, J.-L. Li, M. J. McAllister, H. Sai, M. Herrera-Alonso, D. H. Adamson, R. K. Prud'homme, R. Car, D. A. Saville, I. A. Aksay, *J. Phys. Chem. B* **2006**, *110*, 8535 – 8539; b) M. J. McAllister, J.-L. Li, D. H. Adamson, H. C. Schniepp, A. A. Abdala, J. Liu, M. Herrera-Alonso, D. L. Milius, R. Car, R. K. Prud'homme, I. A. Aksay, *Chem. Mater.* **2007**, *19*, 4396 – 4404.
[6] a) W. Zhang, M. Dubois, K. Guérin, P. Bonnet, E. Petit, N. Delpuech, D. Albertini, F. Masin, A. Hamwi, *Carbon* **2009**, *47*, 2763 – 2775; b) N. D. Leifer, V. S. Johnson, R. Ben-Ari, H. Gan, J. M. Lehnes, R. Guo, W. Lu, B. C. Muffoletto, T. Reddy, P. E. Stallworth, S. G. Greenbaum, *J. Electrochem. Soc.* **2010**, *157*, A148 – A154.
[7] a) D. Sheppard, R. Terrell, G. Henkelman, *J. Chem. Phys.* **2008**, *128*, 134106 – 134110; b) G. Kresse, J. Furthmüller, *Comput. Mater. Sci.* **1996**, *6*, 15 – 50; c) G. Kresse, D. Joubert, *Phys. Rev. B* **1999**, *59*, 1758 – 1775.
[8] L.-M. Liu, R. Car, A. Selloni, D. M. Dabbs, I. A. Aksay, R. A. Yetter, *J. Am. Chem. Soc.* **2012**, *134*, 19011 – 19016.
[9] a) S. Mao, H. Pu, J. Chen, *RSC Adv.* **2012**, *2*, 2643 – 2662; b) J. M. Carlsson, M. Scheffler, *Phys. Rev. Lett.* **2006**, *96*, 046806; c) B. Sanyal, O. Eriksson, U. Jansson, H. Grennberg, *Phys. Rev. B* **2009**, *79*, 113409.
[10] G.-D. Lee, C. Z. Wang, E. Yoon, N.-M. Hwang, K. M. Ho, *Phys. Rev. B* **2006**, *74*, 245411.
[11] Z. Wang, Y. G. Zhou, J. Bang, M. P. Prange, S. B. Zhang, F. Gao, *J. Phys. Chem. C* **2012**, *116*, 16070 – 16079.
[12] a) K. N. Kudin, B. Ozbas, H. C. Schniepp, R. K. Prud'homme, I. A. Aksay, R. Car, *Nano Lett.* **2008**, *8*, 36 – 41; b) A. Kaniyoor, S. Ramaprabhu, *AIP Adv.* **2012**, *2*, 032183.
[13] A. J. Valerga, R. B. Badachhape, G. D. Parks, P. Kamarchick, J. L. Wood, J. L. Margrave, U.S. Army Electronics Command, R&D Technical Report, ECOM-0056-F, **1974**.
[14] a) P. Meduri, H. Chen, X. Chen, J. Xiao, M. E. Gross, T. J. Carlson, J.-G. Zhang, Z. D. Deng, *Electrochem. Commun.* **2011**, *13*, 1344 – 1348; b) S. S. Zhang, D. Foster, J. Read, *J. Power Sources* **2009**, *188*, 601 – 605.
[15] D. M. Ceperley, B. J. Alder, *Phys. Rev. Lett.* **1980**, *45*, 566 – 569.
[16] J. M. Soler, E. Artacho, J. D. Gale, A. García, J. Junquera, P. Ordejón, D. Sánchez-Portal, *J. Phys. Condens. Matter* **2002**, *14*, 2745 – 2779.
[17] N. Troullier, J. L. Martins, *Phys. Rev. B* **1991**, *43*, 1993 – 2006.

Received: October 7, 2014
Revised: November 27, 2014
Published online on February 12, 2014

© 2014 Wiley-VCH Verlag GmbH & Co. KGaA, Weinheim